

Cite this: *J. Mater. Chem. B*, 2022, 10, 3876

A lipidic mesophase with tunable release properties for the local delivery of macromolecules: the apoferritin nanocage, a case study†

Oumar Elzenaty, Paola Luciani  and Simone Aleandri *

Lipid mesophases are able to incorporate and release a plethora of molecules, spanning from hydrophobic drugs to small hydrophilic proteins and therefore they have been widely used as drug delivery systems. However, their 3–5 nm water channels do not allow the release of large hydrophilic molecules such as monoclonal antibodies and therapeutic proteins. To overcome this major geometrical constraint, we designed a gel by mixing monoacylglycerol lipids, generally recognized as safe for human and/or animal use by FDA, and phospholipids, to obtain a material with swollen water channels suitable to host and further release macromolecules. Apoferritin, a 12 nm nanocage protein with intrinsic tumor-targeting properties able to incorporate several molecules, was selected here as the hydrophilic model protein to be embedded in the biocompatible gel. When immersed completely in the release media, mesophases with a swollen water channel of 22 nm, composed of monoolein and doped with 5 mole% of DOPS and 10 mole% of Chol allowed us to achieve a protein release of 60%, which is 120 times higher with respect to that obtained by employing non swollen-LMPs composed only of monoolein. Thus, the formulation can be administered locally to the rectal or vaginal mucosa, reducing the drawbacks often associated with the parenteral administration of bio-therapeutics. This approach would pave the way for the local application of other biomacromolecules (including human ferritin, monoclonal antibodies and antibody drug-conjugates) in those diseases easily reachable by a local application such as rectal or vaginal cancer.

Received 23rd February 2022,
Accepted 11th April 2022

DOI: 10.1039/d2tb00403h

rsc.li/materials-b

Introduction

Parenteral administration of therapeutic proteins is the fastest way to ensure their high bioavailability, either in cancer or in inflammation therapy; however this administration route is often associated with inconvenient side effects such as immune reactions, organ-specific adverse events and low patient compliance.¹ Although different drug delivery approaches have been employed to alleviate these disadvantages, toxicity, unsatisfactory response rate, and low tissue-specificity and selectivity still pose an issue.² An efficient strategy to develop more efficacious and safer therapies aims at exploiting local administration routes such as rectal, vaginal, ocular, intranasal and buccal through which the therapeutic proteins can be delivered directly to the tumor or inflammation site with minimal exposure of distant (healthy) tissues, thus reducing the drug

side effects.³ Enemas, foams and creams as a basic form of local drug delivery systems are routinely used in ulcerative colitis to administer small molecules^{4,5} whereas different drugs have been embedded in vaginal ring and administered into the cervicovaginal tract.^{6–9} While rings and other implants cause discomfort to the patient, liquid like formulations (such as enema) do not remain in the administration site for enough time to guarantee adequate drug absorption. However, foam and ointments do not effectively reach remote tissue areas.⁵ Thus, improving the local dosage form efficacy using a suitable non-invasive drug delivery system not only could solve the current shortcomings associated with existing therapies involving small molecules, but also would allow local administration of biotherapeutics. Lipidic mesophases (LMPs) constitute an attractive platform able to deliver locally hydrophilic biomacromolecules and protect them from chemical and physical degradation *in vivo*.¹⁰ Interestingly, LMPs have been recently used to avoid protein denaturation after oral administration¹¹ since the lipid structure maintains the correct conformation of proteins.¹²

Upon hydration, monoacylglycerol lipids (generally recognized as safe for human and/or animal use by FDA) can form

Department of Chemistry, Biochemistry and Pharmaceutical Sciences, University of Bern, Bern, Switzerland. E-mail: simone.aleandri@unibe.ch

† Electronic supplementary information (ESI) available. See DOI: <https://doi.org/10.1039/d2tb00403h>



lamellar, hexagonal and cubic phases (with *Ia3d*, *Pn3m* or *Im3m* crystallographic space groups).^{13–15} Each phase has its own rheological behavior, which varies tremendously because of the diverse topologies of the mesophases. Their viscosity increases progressively from the less viscous lamellar phase to the highly elastic bicontinuous cubic phases. These properties make LMPs particularly suitable for vaginal administration, thanks to the mucoadhesivity of the gel and the possibility of controlling the delivery of small and large hydrophilic drugs. Indeed, the release rate of drugs incorporated into the LMPs can be regulated by tuning either the size of the aqueous channels¹⁶ or the symmetry of the mesophase.^{17–19} LMP based-gels can be utilized as a platform to encapsulate and deliver locally a plethora of different molecules, including small hydrophilic proteins.^{12,20–24} However, typical LMPs have water channels with a diameter of 3–5 nm and this geometric constraint does not allow the release of large hydrophilic protein such as ovalbumin, apoferritin, and DNA.²⁵ Pioneering works to overcome this major structural limitation employed octyl glucoside to modify the monoglyceride based mesophases and obtain a large *Pn3m* cubic phase with swollen water channels.^{26,27} Further attempts have been done by incorporation in LMPs of a series of additives including sucrose stearate, cholesterol, neutral lipids and charged phospholipids.^{28–35}

Inspired by these approaches, within this work 1, 2-dioleoyl-*sn*-glycero-3-phospho-(1'-*rac*-glycerol) (DOPG), 1,2-dioleoyl-*sn*-glycero-3-phospho-l-serine (DOPS) and 1, 2-dioleoyl-3-trimethylammonium propane (DOTAP) were added together with cholesterol (Chol) to a monoolein/water system to form a stable ultra-swollen cubic phase able to host and release a big macro molecule without disrupting the 3D structure of the gel. Small angle X-ray scattering (SAXS) and release experiments were used to elucidate how the size of the water channel, the phase identity of the gel and the electrostatic interaction between lipids and protein can be varied to achieve a tunable cargo release. Apoferritin (ApoF), a nanocage protein with a diameter of 12 nm, has been selected here as hydrophilic model protein to be embedded in our gel. ApoF is a nanocarrier able to incorporate several anticancer toxins and it is reported to have intrinsic tumor-targeting properties through the binding to its receptor (transferrin receptor 1, Tfr1), overexpressed on tumor cells.^{36–40} The potentiality of this delivery systems are nowadays also exploited by Thena Biotech S.r.l., an Italian Pharma Company that has developed and patented a novel human ferritin (HfT) cage containing peptides that improves the protein performance *in vivo*.^{38,39} However, a major limitation is that Apoferritin and HfT must be administered by parenteral injection (intravenous in most of the cases) and, despite their high tumour selectivity, they might be taken up also by healthy tissues (due to the intrinsic and ubiquitous need for iron in human cells), worsening the treatment's side effects. To overcome this issue and administer ApoF locally, we aimed at engineering a highly swollen biocompatible cubic phase able to release the cargo protein only in the proximity of the needed site, reducing the side effects and the drawbacks associated with a parenteral administration. This approach can pave the

way for the local application of other biomacromolecules (including HfT, mAb and antibody–drug conjugates; ADC) to treat diseases in organs easily reachable by a local application, such as rectal or vaginal cancer.

Results and discussion

LMPs can generally entrap proteins and release them after a certain time.^{20,41,42} However, while small hydrophilic biomolecules such as lysozyme are known to be released during a period of hours by virtue of their smaller size compared to the gel water channel dimension (d_w), ApoF (a 12 nm nanocage) being larger than the gel channel (3–5 nm) and somewhat surface active protein (with a negative zeta potential of -13 mV), appears to be retained in the MO based LMPs for a period of weeks.²⁵ When these protein loaded-gels are administered locally, such a slow release rate is not suitable, since it is not feasible for a patient to retain the formulation (into the rectum or into vagina) for days. Therefore, this limitation has to be overcome and a faster release rate needs to be achieved. An interesting approach is provided by Kozaka *et al.*,⁴³ who formulated swollen LMPs (with channel of *ca.* 6 nm) using *N*-acetyl-octyl-glucoside able to release 70% of octreotide (radius of gyration, R_g , of 7.14 Å) and 40% of lysozyme (R_g of 14.8 Å) after 24 h. However, also in this case only 1% of bovine serum albumin (R_g of 27.6 Å) was released from the swollen gel.

Differently, within this work we incorporated a series of charged phospholipids (DOPS, DOPG and DOTAP) achieving an adequate and tunable ApoF release rate. The anti-inflammatory activity of DOPS, DOPG⁴⁴ and DOTAP⁴⁵ is of benefit to the proposed local formulations and was a deciding factor in our choice to use these lipids over other reported swelling agents. We envisage that the anti-inflammatory activity could be preserved and potentially synergistically augmented in the lipidic cubic phase, as these formulations would deliver both anti-inflammatory lipids and a therapeutic protein.

The utilization of LMPs as protein carriers requires a comprehensive understanding and control of their physicochemical properties. For this purpose, in this study SAXS was used to systematically investigate the gel design space of the MO-based cubic structure of ApoF-free gels, as well as LMPs loaded with ApoF. In agreement with the literature and as shown in Fig. 1, the addition of DOPS and DOPG to the MO based system induces a cubic-*Pn3m*-to-cubic-*Im3m*-phase transition,⁴⁶ while the addition of DOTAP induces a cubic-*Pn3m*-to-cubic-*Ia3d*-phase transition.⁴⁷ The difference in lattice parameters obtained between DOPS and DOPG was justified by taking into account the higher ability of serine to form hydrogen bonding interactions with respect to the glycerol head group. This explains why DOPS enriched gel forms most curved structure with the highest lattice.⁴⁶

On the other hand, the addition of Chol (5 and 10% mole) to the MO/water system leads to an increase of the lattice (99 and 110 Å, respectively) without affecting the gel phase identity which is *Pn3m* throughout (see also the ESI,[†] Table S1).



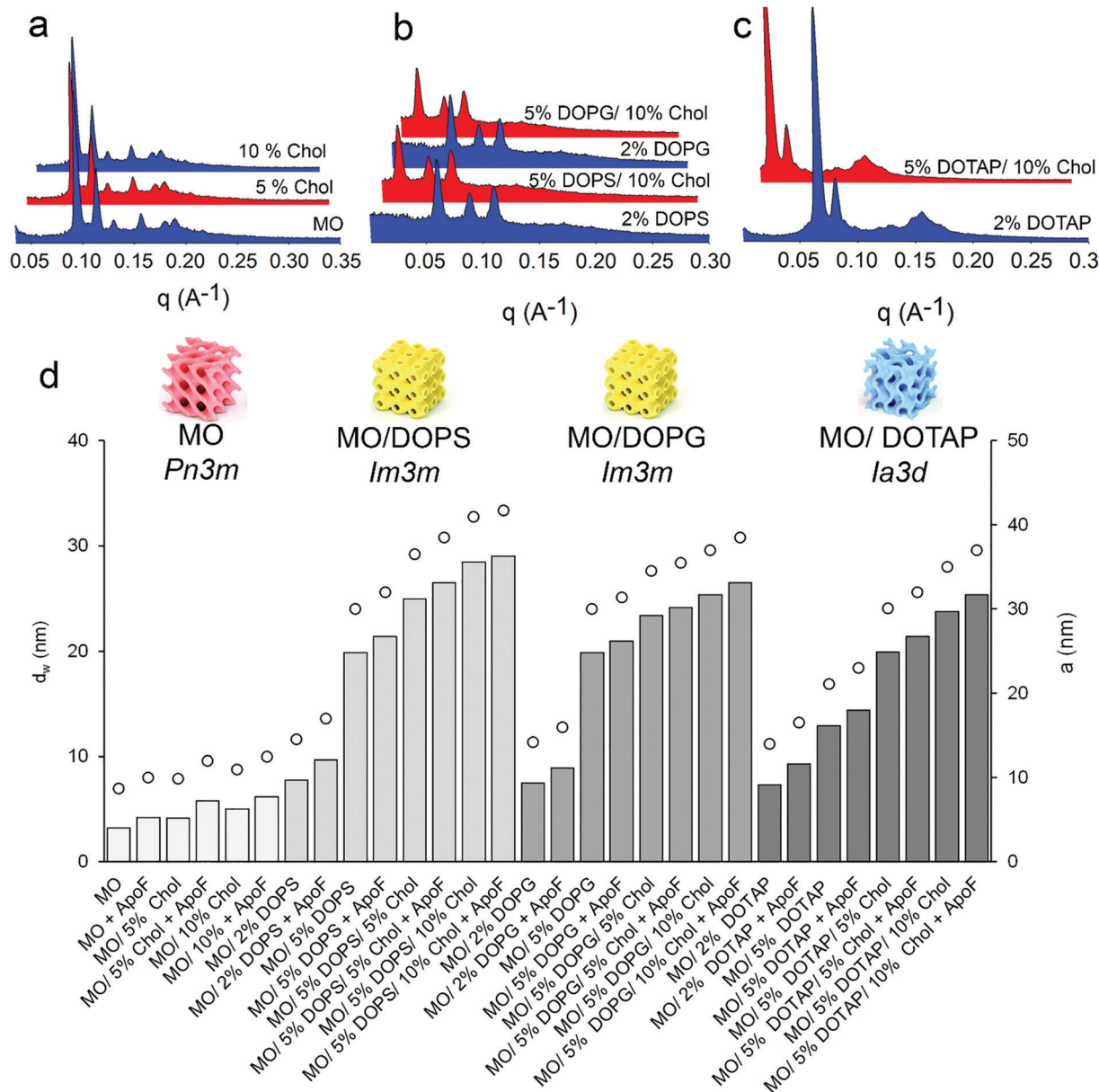


Fig. 1 Representative SAXS spectra (Panels a, b and c) of the ApoF-loaded gels composed by MO (a); MO/DOPS or MO/DOPG (b); and MO/DOTAP (c). Obtained structural parameters from SAXS experiments are summarized in Panel d. Water channel dimension (d_w) is reported as bar plots (left axis) whereas lattice parameters (a) are reported as white circles (right axis). All the formulations were measured at 37 °C in excess of the aqueous phase (70% w/w), the amount of DOPS, DOPG, Chol and DOTAP are reported as molar percentage while the protein loaded samples (+ApoF) contain 1% w/w of protein (1 mg/100 mg gel).

In addition, Chol also augments the swelling of the *Im3m* and *Ia3d* geometry obtained in the presence of DOPS, DOPG and DOTAP, respectively. Chol in the formulation acts as a stiffening agent and it keeps the fluid bilayer stable.⁴⁸ Thanks to its activity, the mesophases can be further swollen by means of anionic lipids, allowing us to achieve lattice parameters comparable with those reported in the literature.^{34,49,50}

In all formulations, independently from their geometry, the 3D structure flexibility of the liquid crystal allows accommodation of the oversized additive and thus, once embedded, the ApoF is able to swell the LMPs water channel of *Pn3m*, *Im3m*

and *Ia3d* symmetry of *ca.* 2–4 nm by itself (see Fig. 1 and ESI,† Table S1). This finding is in agreement with other reported investigations performed in excess of water showing that the embedded transferrin increases the cubic lattice without modification of the space group.⁵¹ Interestingly, the addition of the soluble protein, at least at the level used, does not affect the phase identity of the MO/water system, which is *Pn3m* throughout. This observation is not in agreement with a previous publication,²⁵ where ApoF induced a *Pn3m* to *Im3m* phase transition; however, in that case the transition was observed only at the end of the ApoF release experiment which took several weeks. Moreover, it has to



be mentioned that in this work a low protein to lipid ratio was employed (1 mg protein/30 mg lipid or 1 mg protein/100 mg gel). At least at the used experimental condition the amount of embedded ApoF is not enough to induce any phase change. However, increasing the protein to lipid ratio (as in the case of LMPs dispersion, *i.e.*, cubosomes) induces the above-mentioned structural effect.⁵²

It has been also reported that the presence of big macromolecules such as polysaccharide in the MO/water system induce a phase transition (from *Ia3d* to *Pn3m*), promoting structures with larger water channels.⁵³

All SAXS measurements and the release experiments were carried out above the gels' maximum hydration level, beyond which the gel cannot swell anymore and the excess of water is confined outside the bicontinuous structure (see the ESI,† Table S2). Although under these circumstances the structural parameters of the phases are not limited by the available solvent,⁵⁴ a portion of ApoF might be confined outside the

LMPs, too. For these reasons, the protein entrapment efficacy (EE%) was evaluated and linked to the d_w , and thus to the hydration capacity (water intake) of the systems. As shown in Fig. 2, increasing the dimension of the water channel (d_w , reported as black circles) increases the amount of a water uptake (reported as black squares) into the gel structure and in turn the encapsulation of the protein (see also the ESI,† Table S2). Formulations with a d_w of *ca.* 5 nm and a corresponding water intake of *ca.* 40% granted an EE% of maximum 70%. If the d_w increases, the gel can incorporate more aqueous phase, and hence more protein. As a consequence, the highest EE% was obtained with the formulation containing 5% DOPS and 10% Chol (d_w of *ca.* 22 nm) while a further increase of DOPS (10%) led to the formation of a mixed phase (*Im3m* + L phase; result not shown).

Interestingly, whereas there is a correlation between the aqueous channel size and the EE% among the formulations containing DOPS and DOPG (with an *Im3m* symmetry), in the

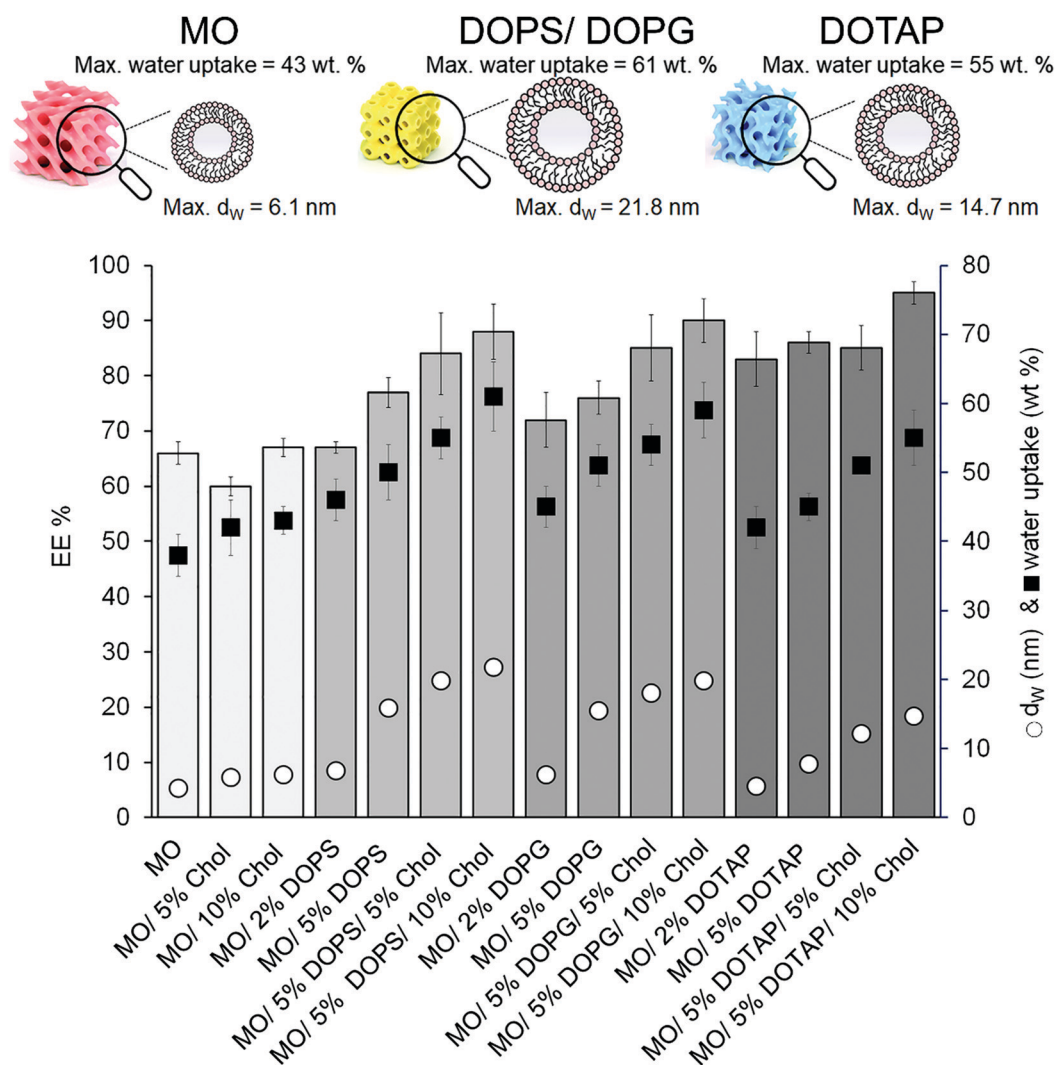


Fig. 2 ApoF entrapment efficacy (EE%, reported as bar plot – left axis) in the gels, water channel dimension (d_w) reported as white circles and water uptake reported as black squares (right axis). All the formulation are in excess of water (hydrated with 70% w/w solution containing 1% w/w of protein), the amount of DOPS, DOPG, Chol and DOTAP are reported as molar percentage. Mean \pm standard deviation (SD) ($n = 3$).



case of formulations containing DOTAP (with an *Ia3d* symmetry) the EE% seems to be independent from d_w , and in any case higher than those obtained with negatively charged lipids. Although the DOTAP-doped formulations have a maximum hydration level (and thus a d_w) comparable with their counterpart obtained with DOPS/DOPG, the EE% achieved with these gels is higher. This phenomenon can be explained by taking into account the electrostatic interaction between ApoF (negatively charged; with a zeta potential of -13 mV) and the positively charged DOTAP. This interaction was already shown to be effective in sequestration of positively charged molecules from the environment into negatively LMPs.⁵⁵ Moreover, the attractions between the positively charged doxorubicin and the negatively charged LMPs doped with anionic lipid was used to enhance the encapsulation and thus the binding of the drug in the gel matrix.⁵⁶ Our results are in agreement with these studies and in the case of the formulation composed of 5% DOTAP and 10% Chol the combination of swollen channel of *ca.* 16 nm and electrostatic interaction allow the highest EE% of 95% to be reached.

Although a few examples of gel incorporating ferritin are available in the literature, in none of these the release rate can be tuned by controlling the gel composition.^{57–59}

In bicontinuous cubic phases, the drug release is hindered only by the channel size and its tortuosity.⁶⁰ Therefore, the Fickian diffusion processes of hydrophilic molecules is regulated by the symmetry of the cubic mesophase, the size of its aqueous channels and the size of the drug.⁶¹

In the case of LMPs composed by MO/water (with a *Pn3m* geometry and a d_w of 4.2 nm) the ApoF (12 nm) remains lodged in the water channels (see Fig. 3) and only 0.5% is released after 8 h in agreement with the value reported in the literature.²⁵

This very low release rate (but still quantifiable) can be explained taking into account the liquid crystal flexibility,

which creates sections of channels that are large enough to allow the oversized protein to pass through. A similar low diffusion was also obtained by incorporating 5 nm particle inside the water channel of 4 nm in diameter.⁶²

Since the water channels do not exceed the protein diameter, even if the channel dimension is increased either by the presence of Chol (5 or 10%; with a *Pn3m* identity) or by the addition of 2% DOPS/DPG (with an *Im3m* symmetry), the ApoF release remained still low and it reached a maximum of 5% in the case of the formulation containing 2% DOPS (with a d_w of 6.7 nm). As a general rule, the less porous *Im3m* symmetry should show a slower transport efficiency compared with the more porous *Pn3m* geometry.⁶¹ In contrast and somewhat notably, gels having different geometry (*Pn3m* or *Im3m*, obtained by doping the LMP with Chol or DOPS/DOPG, respectively) but similar water channel dimension show the same release percentage demonstrating that the geometry does not influence the diffusion, which is a result of the water channel dimension.

Increasing the amount of the swelling agent (5% DOPS or DOPG) resulted in water channels larger than the embedded protein (15.9 and 15.5 nm, respectively), with a consequent increase of the ApoF diffusion rate. The percentage of cargo released was further augmented increasing the size of water channel using a combination of negatively charged phospholipids and Chol. As shown in Fig. 3.

The highest release was obtained for the gel formulated with 5% of DOPS and 10% Chol, having a water channel of 21.8 nm. When $d_w \gg$ ApoF we did not obtain a complete (100%) protein release. This can be explained firstly considering the short time (and the setup) of our release experiments chosen as a reasonable time for the selected local administration route. The crowded environment created in the aqueous channels of the cubic phase favouring partial protein aggregation during sample preparation or during the release experiments may explain the ApoF partial release. Multimers of 100 nm were also detected in the release media at the end of the experiment (see the ESI;† Fig. S3).

On the other hand, the presence of DOTAP led to an *Ia3d* cubic phase with respect to their counterpart formulations obtained doping LMPs with DOPS or DOPG. The electrostatic interactions between the positively charged lipid (DOTAP) of the hosting gel and the negatively charged protein control the release process. Doping monoglyceride-based LMPs with different molecules to introduce responsive moieties has been already used to actuate a stimuli controlled release, using electrostatic interactions,⁵⁵ whereas positively charged mesophases were also used to retain negatively charged DNA.⁶³ Negrini *et al.* also revealed the general trend that electrostatic attractions between hydrophilic molecules and lipid bilayer always slows down the release rate.⁶⁴

These findings could explain why, even when $d_w >$ ApoF in the case of the LMP composed by 5% DOTAP and 10% Chol, only 13% of the protein is released showing that the electrostatic forces purely govern the diffusion of the protein and it is independent of the water channel dimension and from the

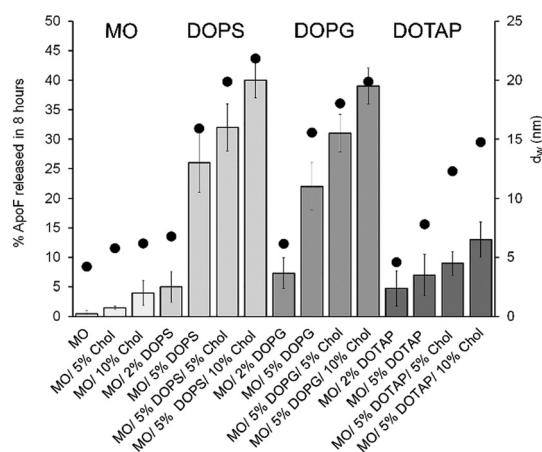


Fig. 3 Percentage of the ApoF released in 8 h from gels reported as the bar plot (left axis) and water channel dimension (d_w) reported as black circles (right axis). All the formulations are in excess of water (hydrated with 70% w/w solution containing 1% w/w of protein), the amount of DOPS, DOPG, Chol and DOTAP are reported as molar percentage. Mean \pm standard deviation (SD) ($n = 3$).



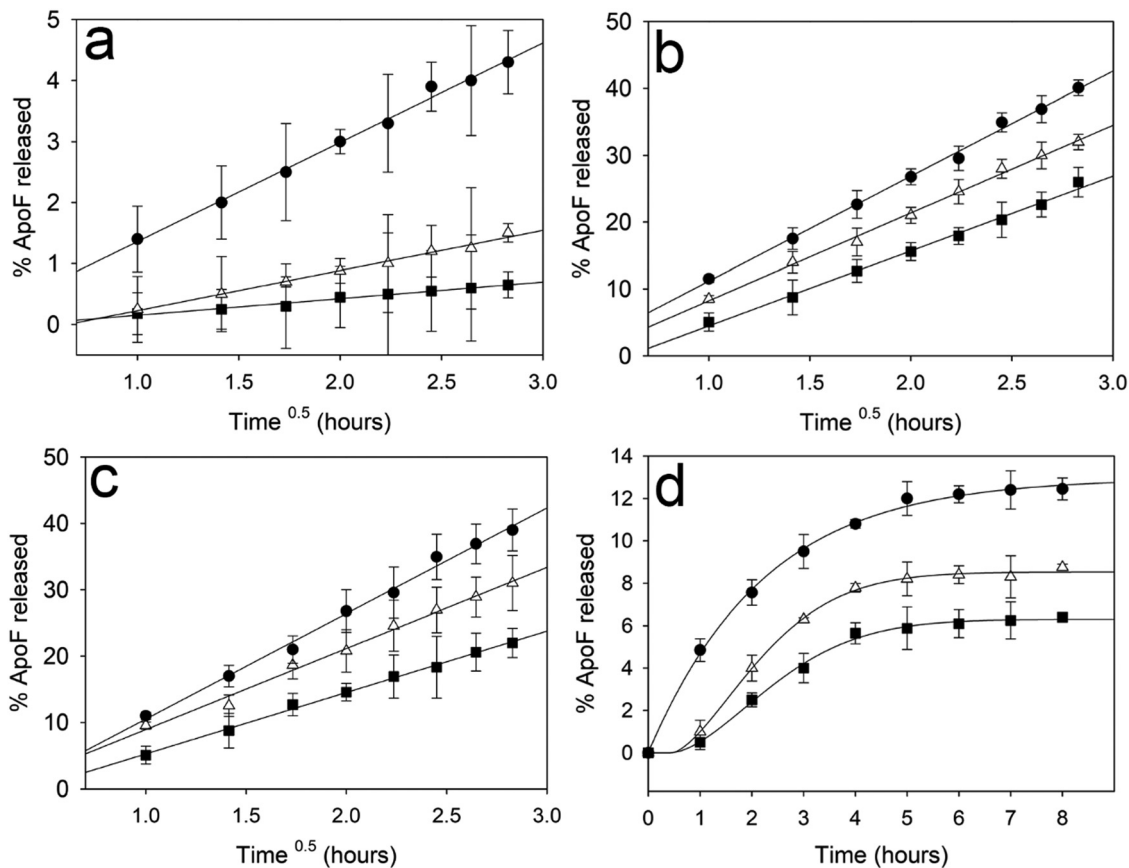


Fig. 4 ApoF release rate after 8 hours from gels composed by MO (a) DOPS (b), DOPG (c) plotted against square root of time ($\text{Time}^{0.5}$ – Higuchi model) and DOTAP (d) plotted against time (Weibull model). In Panel a, the plot shows the release rate obtained with a gel composed by pure MO (black squares); 5% Chol (white triangles) and 10% Chol (black circles). In Panels b–d, the plot shows the release rate obtained with a gel composed of 5% of phospholipids (black squares); 5% of phospholipids and 5% Chol (white triangles) and 5% of phospholipids and 10% Chol (black circles). Mean \pm standard deviation (SD) ($n = 3$). The R^2 obtained for all the fittings are reported in the ESI† (see Table S3 and Fig. S5).

phase identity. Indeed, the release rate achieved from a swollen *Ia3d* gel having a reported water channel of 22.6 nm, composed of monopalmitolein (MP) and distearoyl phosphatidylglycerol (DSPG, neural lipids),³³ is comparable with that obtained for an *Im3m* symmetry (see the ESI†, Fig. S4).

The release of ApoF across the gel was plotted against the square root of time ($t^{0.5}$) and the experimental points were fitted applying the Higuchi equation, which is based on the Fickian diffusion model with a first-order kinetic profile.^{65–67} Although for all the ensuing gels no burst release was observed, while the MO and DOPS/DOPG-doped formulations follow a Fickian diffusion process,²⁸ clearly visible by the linearity of the fittings shown in Fig. 4 (Panels a, b and c), the DOTAP enriched gel (Panel d) deviates from this linearity (see the ESI† Fig. S5 and Table S3). Thus, to fit the experimental data a Weibull model was employed (Fig. 4, Panel d). This model was applied to describe the dissolution of drugs from pharmaceutical formulations and more recently it has been used as an indicator of the mechanism of transport for the drug through the LMPs.⁶⁸

The deviation from a pure diffusive state can be explained by taking into account the forces between the hosting gel and the

protein, as already observed in the case of electrostatic interaction between drug and the mesophases.^{28,64} Interestingly, repulsion (between negatively charged ApoF and DOPS/DOPG) does not affect the release process, which is solely driven by diffusion.

Using the formulation obtained mixing 5% DOPS and 10% Chol (which allow us to achieve the highest ApoF release after 8 h) the EE% and release experiments were performed also with gels hydrated with 50, 70 and 60% w/w aqueous solution containing ApoF *i.e.* below, above and at the maximum hydration level, respectively (see the ESI† Fig. S1). As expected, at the maximum hydration level (60% w/w) all the aqueous phases (which contains the dissolved ApoF) is confined in the gel and thus the entrapment efficacy is the highest ($\text{EE}\% > 98$), whereas the release rate seems to be not affected by the initial water amount (see the ESI† Fig. S6).

The ApoF release for this formulation was carried out also in a peyorative condition where more surface area of the gel was exposed to the release medium. In this setup (see the ESI† release experiment using a basket), the gel was completely immersed in the release medium and the protein can diffuse out of the gel in all directions (named 3D in Fig. 5), while in the



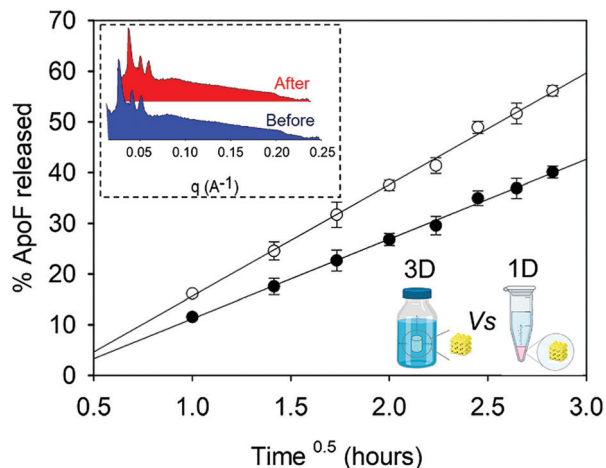


Fig. 5 ApoF release rate from gels composed by MO and doped with 5% DOPS and 10% Chol plotted against square root of time using the 1D (black circles) or 3D (white circles) release set up. Mean \pm standard deviation (SD) ($n = 6$). The diffusion coefficients ratio (D_{3D}/D_{1D}) is obtained by the ratio between the slopes of the linear regression obtained for the 1D and 3D release experiments. The SAXS spectra before and after the release experiment (3D) is shown in the inset.

conventional setup (named 1D) the cargo was allowed to leave the gel only by diffusing in one direction, *i.e.* from the mesophases into the overlay. After the release experiment, the gel was extracted from the basket and measured by SAXS as described in the method section. As expected, the phase identity of the gel does not change after the release experiment (see the inset in Fig. 5) and the diffusion coefficient obtained in the case of 1D setup is 1.9 time lower than that obtained in the case of 3D release.

All the above-described characterizations suggest that the ensuing DOPS enriched-gel can be the optimal candidate for a local administration of biotherapeutics. Besides the physico-chemical properties of the gel prompting a release profile suitable for a mucosal application, the presence of a positively charged protein (such as transferrin) on the damaged epithelial surface can provide a molecular target for drug carriers with negative surface charge.^{3,69,70} As a result, the binding of the LMPs to the mucosa could prolong local drug availability and permit a reduction in dosing frequency.

From a rheological point of view, the swollen gel and the MO-based LMP show a viscoelastic behaviour where the elastic modulus dominates ($G' > G''$; see ESI,† Fig. S7). However, whereas the transition-to-flow regions is not visible for the MO-based gel, a low-frequency crossover is indeed observed in the frequency range considered for the DOPS enriched formulation. These observations are in agreement with those already reported in the literature,⁷¹ according to which DOPS and Chol render the lipidic bilayer more fluid. As a result, the gel starts acting as a viscous fluid and it has a low structural strength, resulting in a less viscous formulation easier to administer and able to treat remote tissue areas. On the other hand, the ensuing gel has a viscosity higher than the commercially available enemas.^{15,72,73}

Conclusions

Using phospholipids to enlarge the water channels of bicontinuous cubic phases and Chol which keeps stable the fluid bilayer, we created swollen gels able to host and release the embedded ApoF. This safe and easy-to-manufacture release system could serve as a versatile platform to encapsulate biomacromolecules and it paves the way for the mucosal application of ApoF and other biomacromolecules including HfT, mAb and antibody–drug conjugates in diseases such as rectal and vaginal tumors, that are easily reachable by local administration, reducing the systemic drawbacks associated with a parenteral administration.

The use of such a gel could allow the patient to apply the formulation similarly to an enema or a vaginal irrigation; yet, differently from pharmaceutical solutions, the viscous gel could initiate a sustained local protein release decreasing dosing frequency and improving patient compliance.

Experimental section

Materials

Dimodan MO 90D was gifted by Danisco (Denmark) and was used as received. This commercial-grade form contains more than 90 wt% monoolein (MO). 1,2-Dioleoyl-*sn*-glycero-3-phospho-(1'-*rac*-glycerol) (DOPG) and 1,2-dioleoyl-*sn*-glycero-3-phospho-L-serine (DOPS) was kindly provided by LIPOID (Ludwigshafen, Germany). 2-Dioleoyl-3-trimethylammonium propane (DOTAP) was purchased from Merck (Darmstadt, Germany). Apoferritin (ApoF) was purchased from MP Biomedicals (Irvine, CA USA). Cholesterol (Chol; Grade $\geq 99\%$) and PBS tablets (one tablet in 1 L of deionized H₂O yields 140 mM NaCl, 10 mM phosphate buffer, and 3 mM KCl, pH 7.4 at 25 °C.) were purchased by Sigma Aldrich. Ultrapure water of resistivity 18.2 M Ω .cm was produced by Barnstead Smart2pure (Thermo Scientific) and used as the aqueous phase. Chloroform was obtained from Fisher Scientific (Schwerte, Germany).

Mesophase sample preparation

Dimodan MO 90D was used as the main lipid constituent of the mesophases and doped with 0, 2 or 5 mole% of DOPS, DOPG or DOTAP and formulated with 0, 5 or 10 mole% of Chol (total lipid amount: 30 mg). Lipidic mixtures were prepared by co-dissolving the appropriate volume amounts of lipids stock solutions in chloroform. Solvent was then completely removed under reduced pressure (lyophilization for 24 h at 0.22 mbar) and the obtained dried lipid mixture were hydrated by mixing weighed quantities (70 mg) of water inside sealed Pyrex tubes by vortexing at room temperature until a homogenous mixture was obtained. The mesophase was then allowed to equilibrate at 37 °C for 72 h in the dark. In the case of ApoF-loaded samples, the obtained lipid mixtures were hydrated with a protein solution (freshly prepared) in water achieving 1% w/w of ApoF-loaded gel (1 mg ApoF/100 mg gel). All the samples coexist with excess water so that their structural parameters are not limited by the available solvent. A list of the produced



formulations together with their structural parameters are reported in the ESI† (see Tables S1 and S2).

Small angle X-ray scattering

SAXS measurements were used to determine the phase identity and symmetry of the produced LMPs. Measurements were performed on a Bruker AXS Micro, with a microfocused X-ray source, operating at a voltage and filament current of 50 kV and 1000 μ A, respectively. The Cu K α radiation ($\lambda_{\text{Cu K}\alpha} = 1.5418 \text{ \AA}$) was collimated by a 2D Kratky collimator, and the data were collected by a 2D Pilatus 100 K detector. The scattering vector $Q = (4\pi/\lambda) \sin \theta$, with 2θ being the scattering angle, was calibrated using silver behenate. Data were collected and azimuthally averaged using the Saxsgui software to yield 1D intensity *vs.* scattering vector Q , with a Q range from 0.001 to 0.5 \AA^{-1} . For all measurements the samples were placed inside a stainless-steel cell between two thin replaceable mica sheets and sealed by an O-ring, with a sample volume of 10 μ L and a thickness of ~ 1 mm. Measurements were performed at 37 $^{\circ}\text{C}$, and samples were equilibrated for 10 min before measurements, whereas scattered intensity was collected over 30 min. To determine the structural parameters such as the size of the water channels, SAXS data information on the lattice were combined with the composition of the samples. Triply periodic minimal surfaces arguments⁷⁴ were used to estimate the diameter of the water channel for the bicontinuous cubic phases (*Ia3d*, *Pn3m*, and *Im3m*). Briefly, following determination of the lattice parameter (a) using SAXS data and assuming that the fixed lipid volume fraction, ϕ , and the geometry of the system remain constant, the diameter of aqueous channels (d_w) and the length of lipid chains (L_{lip}) can be calculated according to Mezzenga *et al.*¹⁵ (all the equations and parameters used are described in the ESI†).

SAXS measurements were also used to measure LMPs composed by Dimodan MO 90D, 5 mole% of DOPS, 10 mole% of Chol and hydrated using different amount of aqueous phase (45, 50, 55, 60, 62, 65 and 70% w/w). Increasing the water amount, and thereby the hydration of the gel, the Bragg peaks shift at lower q , hence the obtained lattice parameter (a) increases indicating a more swollen water channel. If by increasing the water% in the formulation the lattice does not increase, it means that the formulation reaches its maximum hydration level. Moreover, the maximum hydration level for all the other formulations was estimated by using a gravimetric method as described in the ESI† (Table S2).

ApoF entrapment efficacy and release experiment

On the day of experiment, the tube contains 100 mg of LMP gel was submerged with 2 mL of release medium (PBS at pH 7.4). The tube was shaken gently for 30 s and centrifuged at 1000 $\text{g} \times 60$ s. The supernatant (containing the unencapsulated ApoF) was then removed, transferred into a new Eppendorf tube (named t_0) and analysed to determine the protein entrapment efficacy (EE%). The concentration of the protein was evaluated by fluorescence spectroscopy measuring the fluorescence of tryptophan ($\lambda_{\text{em}} 310$ nm and λ_{ex} at 295 nm) using an Infinite 200 Pro F-Plex plate reader (Tecan, Männedorf, Switzerland)

(see ESI†; Fig. S2).³⁶ After the EE% determination, 2 mL of fresh release medium was added to cover the mesophases and the gel kept at 37 $^{\circ}\text{C}$. The release medium was removed periodically (after 1, 2, 3, 4, 5, 6, 7 and 8 h) for spectroscopic determination of the concentration of ApoF released and replaced with the same volume of fresh solution. The EE% and the percentage of the protein released were calculated from eqn (1) and (2), respectively.

$$\text{EE\%} = [(\text{ApoF}_{\text{TOT}} - \text{ApoF}_{t_0})/\text{ApoF}_{\text{TOT}}] \times 100 \quad (1)$$

$$\% \text{ released} = \{\text{ApoF}_t/[\text{ApoF}_{\text{TOT}} \times (\text{EE\%/100})]\} \times 100 \quad (2)$$

ApoF_{TOT} is the total amount of protein after 100% release, ApoF_{t_0} is the amount of protein in the t_0 sample, and ApoF_t is the protein amount released during the experiment. The % of protein released after 8 h was then calculated for each formulation and reported in Fig. 3, whereas the % of cumulative ApoF release was plotted *versus* the time in Fig. 4. The release experiments were also carried out also in a pejorative condition where more surface area of the gel was exposed to the release medium (see ESI† Release experiment using a basket).

Author contributions

Oumar Elzenaty: LMPs preparation and release experiments. Paola Luciani: writing – review & editing; project administration; funding acquisition. Simone Aleandri: conceptualization, data curation, methodology, validation, formal analysis, investigation, writing – original draft, visualization.

Conflicts of interest

The authors declare that they have no known competing financial interests or personal relationships that could have appeared to influence the work reported in this paper.

Acknowledgements

Prof. Raffaele Mezzenga (Laboratory of Food & Soft Materials, Institute of Food, Nutrition and Health, IFNH; Department for Health Sciences and Technology, D-HEST, ETH Zurich Switzerland) is acknowledged for his support to conduct the SAXS experiments. Moreover, the authors would like to acknowledge Dr Serena Rosa Alfarano and Ms Francesca Vittorelli for their precious support during the SAXS measurements.

References

- 1 T. T. Hansel, H. Kropshofer, T. Singer, J. A. Mitchell and A. J. T. George, *Nat. Rev. Drug Discovery*, 2010, **9**, 325–338.
- 2 W. C. Chen, A. X. Zhang and S. D. Li, *Eur. J. Nanomed.*, 2012, **4**, 89–93.
- 3 J. Xu, M. Tam, S. Samaei, S. Lerouge, J. Barralet, M. M. Stevenson and M. Cerruti, *Acta Biomater.*, 2017, **48**, 247–257.



- 4 A. Kornbluth and D. B. Sachar, *Am. J. Gastroenterol.*, 2004, **99**, 1371.
- 5 A. Kornbluth and D. B. Sachar, *Am. J. Gastroenterol.*, 2010, **105**, 501–523.
- 6 W. M. Saltzman, J. K. Sherwood, D. R. Adams and P. Haller, *Biotechnol. Bioeng.*, 2000, **67**, 253–264.
- 7 S. Yang, G. Arrode-Bruses, I. Frank, B. Grasperge, J. Blanchard, A. Gettie, E. Martinelli and E. A. Ho, *Sci. Adv.*, 2020, **6**, eabb9853.
- 8 M. Gunawardana, F. Villinger, M. M. Baum, M. Remedios-Chan, T. R. Moench, L. Zeitlin, K. J. Whaley, O. Bohorov, T. J. Smith, D. J. Anderson and J. A. Moss, *Antimicrob. Agents Chemother.*, 2017, **61**(7), e02465–16.
- 9 J. M. Steinbach, *Cell. Mol. Life Sci.*, 2015, **72**, 469–503.
- 10 Nidhi, M. Rashid, V. Kaur, S. S. Hallan, S. Sharma and N. Mishra, *Saudi Pharm. J.*, 2016, **24**, 458–472.
- 11 J. B. Strachan, B. P. Dyett, N. C. Jones, S. V. Hoffmann, C. Valery and C. E. Conn, *J. Colloid Interface Sci.*, 2021, **592**, 135–144.
- 12 A. Zabara, R. Negrini, P. Baumann, O. Onaca-Fischer and R. Mezzenga, *Chem. Commun.*, 2014, **50**, 2642–2645.
- 13 V. Luzzati, A. Tardieu and T. Gulik-Krzywicki, *Nature*, 1968, **217**, 1028–1030.
- 14 S. Aleandri and R. Mezzenga, *Phys. Today*, 2020, **73**, 38–44.
- 15 R. Mezzenga, C. Meyer, C. Servais, A. I. Romoscanu, L. Sagalowicz and R. C. Hayward, *Langmuir*, 2005, **21**, 3322–3333.
- 16 S. Sarkar, N. Tran, S. K. Soni, C. E. Conn and C. J. Drummond, *ACS Biomater. Sci. Eng.*, 2020, **6**, 4401–4413.
- 17 S. Phan, W. K. Fong, N. Kirby, T. Hanley and B. J. Boyd, *Int. J. Pharm.*, 2011, **421**, 176–182.
- 18 L. M. Antognini, S. Assenza, C. Speziale and R. Mezzenga, *J. Chem. Phys.*, 2016, **145**, 84903.
- 19 S. Phan, W.-K. Fong, N. Kirby, T. Hanley and B. J. Boyd, *Int. J. Pharm.*, 2011, **421**, 176–182.
- 20 J. A. Prange, S. Aleandri, M. Komisariski, A. Luciani, A. Käch, C. D. Schuh, A. M. Hall, R. Mezzenga, O. Devuyst and E. M. Landau, *ACS Appl. Bio Mater.*, 2019, **2**, 2490–2499.
- 21 J. K. Sherwood, L. Zeitlin, X. Chen, K. J. Whaley, R. A. Cone and W. M. Saltzman, *Biol. Reprod.*, 1996, **54**, 264–269.
- 22 W. K. Fong, R. Negrini, J. J. Vallooran, R. Mezzenga and B. J. Boyd, *J. Colloid Interface Sci.*, 2016, **484**, 320–339.
- 23 O. Mertins, P. D. Mathews and A. Angelova, *Nanomaterials*, 2020, **10**.
- 24 S. Aleandri, D. Bandera, R. Mezzenga and E. M. Landau, *Langmuir*, 2015, **31**, 12770–12776.
- 25 J. Clogston and M. Caffrey, *J. Controlled Release*, 2005, **107**, 97–111.
- 26 B. Angelov, A. Angelova, V. M. Garamus, G. Lebas, S. Lesieur, M. Ollivon, S. S. Funari, R. Willumeit and P. Couvreur, *J. Am. Chem. Soc.*, 2007, **129**, 13474–13479.
- 27 B. Angelov, A. Angelova, M. Ollivon, C. Bourgaux and A. Campitelli, *J. Am. Chem. Soc.*, 2003, **125**, 7188–7189.
- 28 R. Negrini and R. Mezzenga, *Langmuir*, 2012, **28**, 16455–16462.
- 29 A. Angelova, B. Angelov, R. Mutafchieva, V. Garamus, S. Lesieur, S. Funari, R. Willumeit and P. Couvreur, in *Prog. Colloid Polym. Sci.*, 2011, vol. 138, pp. 1–6.
- 30 V. Cherezov, J. Clogston, Y. Misquitta, W. Abdel-Gawad and M. Caffrey, *Biophys. J.*, 2002, **83**, 3393–3407.
- 31 H. M. G. Barriga, A. I. I. Tyler, N. L. C. McCarthy, E. S. Parsons, O. Ces, R. V. Law, J. M. Seddon and N. J. Brooks, *Soft Matter*, 2015, **11**, 600–607.
- 32 A. I. I. Tyler, H. M. G. Barriga, E. S. Parsons, N. L. C. McCarthy, O. Ces, R. V. Law, J. M. Seddon and N. J. Brooks, *Soft Matter*, 2015, **11**, 3279–3286.
- 33 A. Zabara, J. T. Y. Chong, I. Martiel, L. Stark, B. A. Cromer, C. Speziale, C. J. Drummond and R. Mezzenga, *Nat. Commun.*, 2018, **9**, 544.
- 34 J. Borné, T. Nylander and A. Khan, *Langmuir*, 2001, **17**, 7742–7751.
- 35 M. Mendozza, A. Balestri, C. Montis and D. Berti, *Int. J. Mol. Sci.*, 2020, **21**, 1–16.
- 36 N. Song, J. Zhang, J. Zhai, J. Hong, C. Yuan and M. Liang, *Acc. Chem. Res.*, 2021, **54**, 3313–3325.
- 37 J. Zhang, D. Cheng, J. He, J. Hong, C. Yuan and M. Liang, *Nat. Protoc.*, 2021, **16**, 4878–4896.
- 38 E. Falvo, E. Tremante, R. Fraioli, C. Leonetti, C. Zamparelli, A. Boffi, V. Morea, P. Ceci and P. Giacomini, *Nanoscale*, 2013, **5**, 12278–12285.
- 39 E. Falvo, E. Tremante, A. Arcovito, M. Papi, N. Elad, A. Boffi, V. Morea, G. Conti, G. Toffoli, G. Fracasso, P. Giacomini and P. Ceci, *Biomacromolecules*, 2016, **17**, 514–522.
- 40 E. Falvo, F. Malagrinò, A. Arcovito, F. Fazi, G. Colotti, E. Tremante, P. Di Micco, A. Braca, R. Opri, A. Giuffrè, G. Fracasso and P. Ceci, *J. Controlled Release*, 2018, **275**, 177–185.
- 41 J. Clogston and M. Caffrey, *J. Controlled Release*, 2005, **107**, 97–111.
- 42 S. B. Rizwan, D. Assmus, A. Boehnke, T. Hanley, B. J. Boyd, T. Rades and S. Hook, *Eur. J. Pharm. Biopharm.*, 2011, **79**, 15–22.
- 43 S. Kozaka, R. Wakabayashi, N. Kamiya and M. Goto, *ACS Appl. Mater. Interfaces*, 2021, **13**(45), 54753–54761.
- 44 M. E. Klein, S. Mauch, M. Rieckmann, D. G. Martínez, G. Hause, M. Noutsias, U. Hofmann, H. Lucas, A. Meister, G. Ramos, H. Loppnow and K. Mäder, *Nanomedicine*, 2020, **23**, 102096.
- 45 M. C. Fillion and N. C. Phillips, *Br. J. Pharmacol.*, 1997, **122**, 551–557.
- 46 G. Lindblom, L. Rilfors, J. B. Hauksson, I. Brentel, M. Sjölund and B. Bergenstahl, *Biochemistry*, 1991, **30**, 10938–10948.
- 47 C. Leal, N. F. Boussein, K. K. Ewert and C. R. Safinya, *J. Am. Chem. Soc.*, 2010, **132**, 16841–16847.
- 48 D. L. Gater, V. Réat, G. Czaplicki, O. Saurel, A. Milon, F. Jolibois and V. Cherezov, *Langmuir*, 2013, **29**, 8031–8038.
- 49 S. J. Li, Y. Yamashita and M. Yamazaki, *Biophys. J.*, 2001, **81**, 983–993.
- 50 T. S. Awad, Y. Okamoto, S. M. Masum and M. Yamazaki, *Langmuir*, 2005, **21**, 11556–11561.
- 51 A. Angelova, B. Angelov, R. Mutafchieva, S. Lesieur and P. Couvreur, *Acc. Chem. Res.*, 2011, **44**, 147–156.
- 52 A. Angelova, M. Ollivon, A. Campitelli and C. Bourgaux, *Langmuir*, 2003, **19**, 6928–6935.



- 53 R. Mezzenga, M. Grigorov, Z. Zhang, C. Servais, L. Sagalowicz, A. I. Romoscanu, V. Khanna and C. Meyer, *Langmuir*, 2005, **21**, 6165–6169.
- 54 S. S. W. Leung and C. Leal, *Soft Matter*, 2019, **15**, 1269–1277.
- 55 N. Rahanyan-Kagi, S. Aleandri, C. Speziale, R. Mezzenga and E. M. Landau, *Chemistry*, 2015, **21**, 1873–1877.
- 56 E. Nazaruk, E. Górecka, Y. M. Osornio, E. M. Landau and R. Bilewicz, *J. Electroanal. Chem.*, 2018, **819**, 269–274.
- 57 M. K. Shin, S. I. Kim, S. J. Kim, B. J. Kim, I. So, M. E. Kozlov, J. Oh and R. H. Baughman, *Appl. Phys. Lett.*, 2008, **93**, 163902.
- 58 M. K. Shin, G. M. Spinks, S. R. Shin, S. I. Kim and S. J. Kim, *Adv. Mater.*, 2009, **21**, 1712–1715.
- 59 R. Samanipour, T. Wang, M. Werb, H. Hassannezhad, J. M. L. Rangel, M. Hoorfar, A. Hasan, C. K. Lee and S. R. Shin, *ACS Biomater. Sci. Eng.*, 2020, **6**, 277–287.
- 60 I. Martiel, N. Baumann, J. J. Vallooran, J. Bergfreund, L. Sagalowicz and R. Mezzenga, *J. Controlled Release*, 2015, **204**, 78–84.
- 61 S. Assenza and R. Mezzenga, *J. Chem. Phys.*, 2018, **148**, 054902.
- 62 E. Venugopal, S. K. Bhat, J. J. Vallooran and R. Mezzenga, *Langmuir*, 2011, **27**, 9792–9800.
- 63 I. Amar-Yuli, J. Adamcik, S. Blau, A. Aserin, N. Garti and R. Mezzenga, *Soft Matter*, 2011, **7**, 8162–8168.
- 64 R. Negrini, A. Sánchez-Ferrer and R. Mezzenga, *Langmuir*, 2014, **30**, 4280–4288.
- 65 M. Dully, C. Brasnett, A. Djeghader, A. Seddon, J. Neilan, D. Murray, J. Butler, T. Soulimane and S. P. Hudson, *J. Colloid Interface Sci.*, 2020, **573**, 176–192.
- 66 E. Nazaruk, M. Szlezak, E. Gorecka, R. Bilewicz, Y. M. Osornio, P. Uebelhart and E. M. Landau, *Langmuir*, 2014, **30**, 1383–1390.
- 67 R. Negrini and R. Mezzenga, *Langmuir*, 2011, **27**, 5296–5303.
- 68 D. Paolino, A. Tudose, C. Celia, L. Di Marzio, F. Cilurzo and C. Mircioiu, *Materials*, 2019, **12**, 693.
- 69 T. T. Jubeh, Y. Barenholz and A. Rubinstein, *Pharm. Res.*, 2004, **21**, 447–453.
- 70 S. Zhang, J. Ermann, M. D. Succi, A. Zhou, M. J. Hamilton, B. Cao, J. R. Korzenik, J. N. Glickman, P. K. Vemula, L. H. Glimcher, G. Traverso, R. Langer and J. M. Karp, *Sci. Transl. Med.*, 2015, **7**, 1–11.
- 71 C. Speziale, R. Ghanbari and R. Mezzenga, *Langmuir*, 2018, **34**, 5052–5059.
- 72 M. H. Otten, G. de Haas and R. van den Ende, *Aliment. Pharmacol. Ther.*, 1997, **11**, 693–697.
- 73 J. R. Ingram, *Postgrad. Med. J.*, 2005, **81**, 594–598.
- 74 D. C. Turner, Z.-G. Wang, S. M. Gruner, D. A. Mannock and R. N. McElhaney, *J. Phys. II*, 1992, **2**, 2039–2063.

